White Blood Cells Counting Via
Vector Field Convolution Nuclei Segmentation

Simone Porcu, Andrea Loddo, Lorenzo Putzu and Cecilia Di Ruberto

University of Cagliari, Italy

Abstract: Haematological procedures like analysis, counting and classification of White Blood Cells (WBCs) are very helpful in the medical field, in order to recognize a pathology, e.g., WBCs analysis leukaemia correlation. Expert technicians manually perform these procedures, therefore, they are influenced by their tiredness and subjectivity. Their automation is still an open issue. Our proposal aims to replicate every single step of the haematologists' job with a semi-automatic system. The main targets of this work are to decrease the time needed for an analysis and to improve the efficiency of the procedure. It is based on the Vector Field Convolution (VFC) to describe cells edges, going beyond more classic methods like the active contour model. This approach is crucial to face the WBCs clumps and overlaps segmentation issue. To sum up, we defined a system that is able to recognise the leukocytes, to differentiate them from the other blood cells and, finally, to divide the overlapping leukocytes. Experimental results obtained on three public datasets showed that the method is accurate and robust, outperforming the state of the art methods for cells clumps identification and cells counting.

1 INTRODUCTION

Blood is a body fluid deliver. It contains and transports many of the nutrients substances that humans need to live. Blood is mainly composed of two elements: cells and plasma. The blood cells are the red blood cells (RBCs) and white blood cells (WBCs). Haematology is the field related to the study of blood conditions in order to measure the health status of the patients. Nowadays the analysis work flow is a manual process. Every single blood slide is analysed by an expert haematologist that counts and extracts the needed information for the requested analysis. However it is a very delicate procedure and it is error-prone. For this reason, having an automatic or semi-automatic system would be useful to avoid issues. The main contribute of this work is a semi-automated method that can extract all the WBCs from the peripheral blood smear images and count every single WBC in order to obtain their exact count. The proposed system is based on a segmentation algorithm especially designed for this purpose. No machine learning approach has been used in our method, either to increase the performances in detection and to avoid the learning phase, that is slow and focused on a particular training set. Thus the proposed algorithm is not tuned to a specific training set and it could be used for whichever dataset of peripheral blood images. In the literature there are a lot of methodologies devoted to the identification and counting of single cells, but only few works addressed clumped cells separation and counting issues. For this reasons, this work is focused on the clumped cells separation issue. The rest of the paper is organized as follows. Section 2 presents the related works about peripheral blood image analysis. Section 3 illustrates the proposed method. Section 4 presents the obtained results on the considered datasets. Discussions, conclusions and future aspects are finally given in Section 5.

2 STATE OF THE ART

Commonly, blood cells images segmentation can be performed with two different approaches: the first one works at a cell level and the last one aims to do an intra-cell segmentation. The purpose of the first one is to discriminate foreground from background, while the second one has the target to divide the different components contained inside the cells, such as nucleus from cytoplasm or intracellular parasites. For example, Madhloom (Madhloom et al., 2010) imple-

227

mented an automated system to localise and segment WBC nuclei based on arithmetical and threshold operations. Sinha (Sinha and Ramakrishnan, 2003) and Kovalev (Kovalev et al., 1996) tried to differentiate the leukocytes types typically contained in cell images. Sinha used k-means clustering based on the HSV colour space for WBCs segmentation. Kovalev firstly identified the nuclei and then detected the entire membrane by means of region growing techniques. A low-pass filter has been employed (Scotti, 2006) in order to remove background and, after that, WBCs segmentation is approached with different threshold operations and image clustering. Piuri's approach (Scotti and Piuri, 2004) is based on edge detection for WBCs segmentation. Halim (Halim et al., 2011) proposed an automated blast counting method to detect acute leukaemia in blood microscopic images that identifies WBCs through a thresholding operation performed on the S component of the HSV colour space, followed by morphological erosion for image segmentation. Mohapatra (Mohapatra et al., 2013) investigated the early diagnosis of ALL in blood microscopic images. The identification and segmentation of WBCs is realised through image clustering followed by the extraction of different types of features, such as shape, contour, fractal, texture, colour and Fourier descriptors, from the sub-image. Moving to the problem of clumped cells separation, some methods are included in the process of segmentation, while others are specifically dedicated to overlapping cells separation. The Watershed transform is certainly one of the most common methods. Putzu (Putzu et al., 2014) used the distance transform and the watershed algorithm to separate cells agglomerates. The separation is less influenced by cells shape, but it works only for small or simple cells agglomerates. On the other hand, Ghane (Ghane et al., 2017) used K-means algorithm for nuclei segmentation and morphological operators to remove small objects, obtaining an enhancement of the segmentation results. Finally, he used the Watershed transform to split touching cells and nuclei. Mahmood and Alomari (Mahmood et al., 2013), (Alomari et al., 2014), differently from the previous, proposed two WBCs count methods based on the circular Hough transform (CHT). Mahmood applied the CHT on binary images obtained from the Lab colour space, while Alomari modified the CHT in order to reduce the number of cells candidates by choosing the one with the highest probability of being a circle. A different approach has been proposed by Alilou (Alilou and Kovalev, 2013), where a detection phase using grey level co-occurrence matrix has been applied directly on the original images without a previous segmentation. As it can be guessed, it produces

a significant amount of false positives since it works without restrictions on the area of interest. Finally, Di Ruberto (Di Ruberto et al., 2016) and Loddo (Loddo et al., 2016) applied the CHT to recognize circular shapes inside the clumped cells obtained in the segmentation phase. To sum up, every non-classifier based method typically works with the following strategy: first a threshold methodology is used to extract the cells and then the clumped cells separation is realized by using another method, e.g., the Watershed transform. Our work aims to use a different approach. It performs the clumped cells separation along with the segmentation step so that every identified region is obtained in only one computational step.

3 PROPOSED METHOD

The main target of our proposed method is to segment all the WBCs nuclei by using Vector Field Convolution (VFC) strategy and to divide potential clumps by using an analysis of the real cells boundaries, overcoming the use of Watershed transform. The system is composed of the following phases: pre-processing, binary edge map generation, VFC (Bing and Scott, 2007) application, grades transformation, external energy computation, black and white distance calculation and, finally, skeletonizing and region merging application. Figure 1 shows the of proposed method flow diagram. It starts with a contrast stretching on the RGB colour space's G channel. The regions boundaries are extracted by means of a gradient operator which permits to obtain a binary edge map. Subsequently the VFC is computed with the initialization of the kernel vector field and the edge map creation. A first WBCs detection has been so far obtained with the previous steps and a first nuclei segmentation can be consequently obtained by applying the skeleton function on the overlap between the external force and the binary distance transform images. The final segmentation result is described in detail further on.

3.1 Pre-processing

It is the first step of the proposed technique and it is needed to extract all the information for WBCs areas detection. WBCs nuclei has been highlighted by stretching the histogram of RGB colour space's G channel (Figure2). The purpose is to obtain only the cells of interest in order to create the best possible edge map.

The high spacial frequency regions, corresponding to the edges, have been highlighted thanks to the Sobel operator. It is a kind of orthogonal gradient
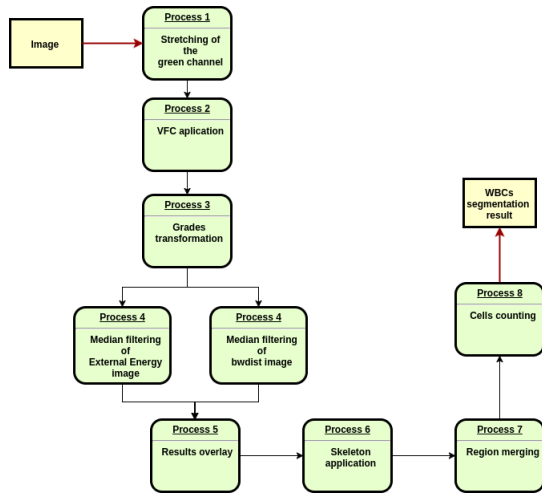
Figure 1: Diagram of WBC image recognizer.

operator and it has the advantage to produce a smoothing effect to the image's random noise (Gao et al., 2010). Gradient corresponds to first derivative, therefore gradient operators are derivative. For a continuous function f (x, y), in the position (x, y), its gradient can be expressed as a vector:

$$\nabla f(x,y) = \begin{bmatrix} G_x & G_y \end{bmatrix}^T = \begin{bmatrix} \dfrac{\delta f}{\delta x} & \dfrac{\delta f}{\delta y} \end{bmatrix} \quad (1)$$

This operator applies two kernels in the two principal directions. Calling G_x and G_y the horizontal and vertical derivative approximations and I the image, the computation is described as follows:

$$G_x = \begin{pmatrix} +1 & 0 & -1 \\ +2 & 0 & -2 \\ +1 & 0 & -1 \end{pmatrix} \times I \quad (2)$$

$$G_y = \begin{pmatrix} +1 & +2 & +1 \\ 0 & 0 & 0 \\ -1 & -2 & -1 \end{pmatrix} \times I \quad (3)$$
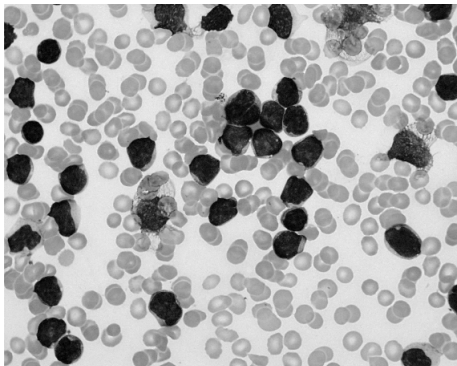

Figure 2: RBC image's G channel extraction. The WBCs are highlighted with respect to the other regions.

where the $\times$ operator indicates the convolution operation.

3.2 VFC Segmentation

An external force, namely the VFC, can be obtained by convolving a vector field with the edge map derived from the image (Bing and Scott, 2007). Active contours using the VFC external force are called VFC snakes. Differently from the GVF (Xu and Prince, 1998) snakes, that are formulated using the standard energy minimization framework, VFC snakes are constructed from a state of equilibrium between the forces. Furthermore, VFC snakes have a lot of advantages, e.g., a wide capture range, they are able to grab the concavities, they are better resistant to noise images, they have the ability to adapt the force field and to reduce drastically the computational cost. Before going into detail, it is useful to define the Vector Field Kernel (VFK). It is computed using the following equation:

$$k(x,y) = m(x,y)n(x,y) \quad (4)$$

where n is the unit vector that points to the origin of the kernel

$$n(x,y) = [\dfrac{-x}{r}, \dfrac{-y}{r}] \quad (5)$$

and m is the magnitude of the vector. Potentially, every single pixel in an image may be attracted to the edge of its region (Bing and Scott, 2007). This fact could be compared to the gravity effect on every single object in Earth: it is attracted to the Earth surface. Consequently, if we consider the origin as the point of interest, VFK has the desirable property that a free particle placed in the vectorial field is able to move to a point of interest. The external force that works in the VFC is defined in this way:

$$f_{vfc}(x,y) = u_{vfc}(x,y), v_{vfc}(x,y) \quad (6)$$

Since the edge map is non-negative and wider near the edges of the image, the VFC acts more on the edges than to homogeneous regions. Therefore, the free particles of homogeneous regions will be attracted to the edges. If we use a complex-valued range, the VFC acts as a filter on the edge map, which does not depend on the origin of the kernel. The VFC field highly depends on the magnitude of the VFK in such a way that it is directly proportional to the VFK(x, y). The farther is the figure of interest (FOI) (Bing and Scott, 2007), the less powerful is the force and, therefore, the magnitude must be expressed as a positive function that decreases with respect to the distance of the origin. Two types of magnitude functions are defined as follows:
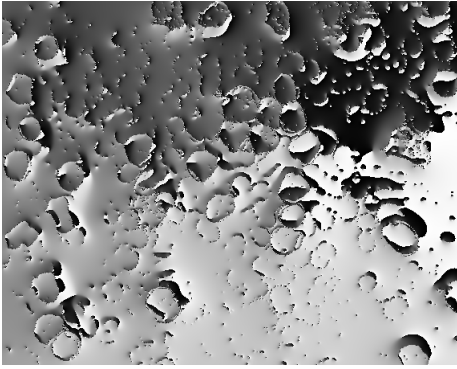
Figure 3: VFC right and left component.

Figure 4: Distance transform image.

$$m_1(x,y) = (r+\varepsilon)^{-\gamma} \qquad (7)$$

$$m_2(x,y) = exp(-r^2\zeta^2) \qquad (8)$$

where γ and ζ are positive parameters to control the decrease rate, ε is a small positive constant which prevents division by zero at the origin, while $m_1(x,y)$ is inspired by Newton's universal gravitation law. Furthermore, the pixels in the edge map can be considered as objects of mass proportional to the strength of the edges and the VFC would be the gravitational field generated by all objects. $m_2(x,y)$ is a Gaussian shape function, and ζ can be viewed as the standard deviation. The influence of FOI is strongly dependent from γ and ζ because it increases if the first one decreases or the second one increases. In general, the influence of FOI should be increased (or decrease) as the signal-to-noise ratio is decreased (or increased) (Bing and Scott, 2007).

The VFC uses the two components of the external force $u_{vfc}(x,y), v_{vfc}(x,y)$ to describe the field of the image and its magnitude. These two components are very useful to describe all the edges, both from single leukocytes and from cell clumps. VFC's right and left components can be computed as follows:

$$u_{vfc} = ExtF(x)/\sqrt{ExtF(x)^2 + ExtF(y)^2} \qquad (9)$$

$$v_{vfc} = ExtF(y)/\sqrt{ExtF(x)^2 + ExtF(y)^2} \qquad (10)$$

where $ExtF$ is the External force of the Field. u and v are two intensity images with values range in $-pi$ and $+pi$. They need to be combined and converted in degrees values so that the orientation of every image pixel can be described, as shown in Fig. 3.

VFC application typically generates some artefacts. In order to delete them all, this method applies the distance transform. It assigns a number that is the distance between each pixel and the nearest non-zero pixel of the image. As a result, the entropy of the image is reduced as well as the noise even though it does not distinguishes if the edge is a RBC's edge or
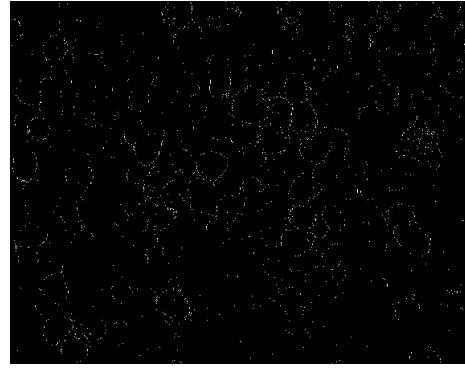
a WBC's edge. As a consequence, the application of the External Energy is needed to overcome this problem.

For an image $I(x,y)$ the general formulation of the image Energy is:

$$E_{image} = w_{line}E_{line} + w_{edge}E_{edge} + w_{term}E_{term} \qquad (11)$$

where $w_{line}, w_{edge}, w_{term}$ are weights of the features.
Line Functional: the line functional, also known as the image intensity, is the attracted value of the dark lines to the light lines. It is possible to choose this value by selecting a positive or negative value of the force

$$E_{line} = filter(I(x,y)) \qquad (12)$$

Edge Functional: The edge functional bases its work on the image gradient.

$$E_{edge} = -|\nabla I(x,y)|^2 \qquad (13)$$

This formula defines the strategy by which the method gets rid of the local minima that are not object of interest. The energy functional using scale space continuation is

$$E_{edge} = -\left|G_\sigma \times \nabla^2 I\right|^2 \qquad (14)$$

where G_σ is a Gaussian with standard deviation σ.
Termination Functional: The lines curvature in an image is used to detect corners and terminations. Put

$$C(x,y) = G_\sigma \times I(x,y) \qquad (15)$$

we derive a gradient angle

$$\theta = \arctan\left(\frac{C_y}{C_x}\right), \qquad (16)$$

the unit vectors that move along the gradient direction

$$\mathbf{n} = (\cos\theta, \sin\theta), \qquad (17)$$

and the unit vectors perpendicular to the gradient direction.

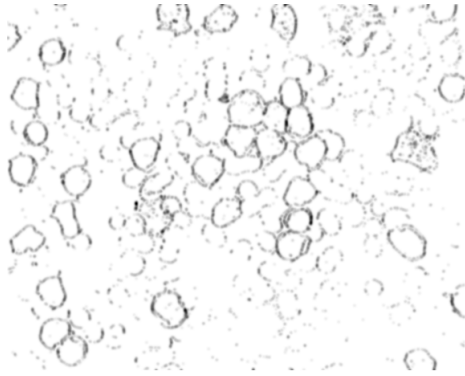$$\mathbf{n}_\perp = (-\sin\theta, \cos\theta). \qquad (18)$$
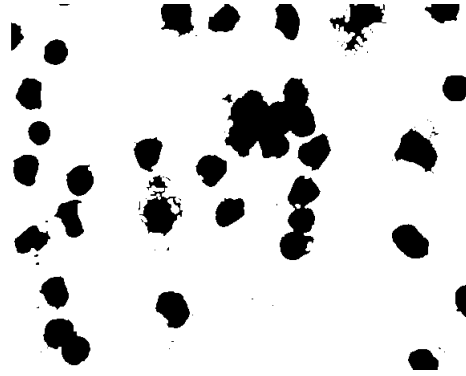
Figure 5: External energy image.
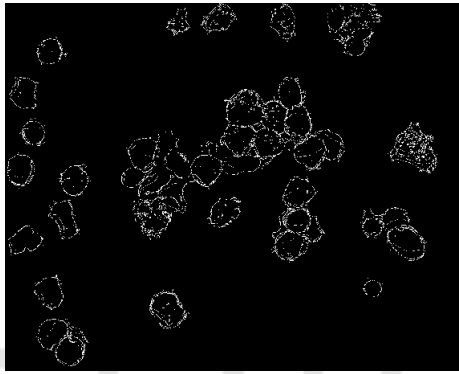

Figure 7: Opened image.

Figure 6: Overlay image.

Having defined the previous four formulas, the termination functional of energy can be defined as follows:

$$E_{term} = \frac{\partial \theta}{\partial n_{\perp}} = \frac{\partial^2 C / \partial^2 n_{\perp}}{\partial C / \partial n} = \\ \Rightarrow \frac{C_{yy} C_x^2 - 2 C_{xy} C_x C_y + C_{xx} C_y^2}{(C_x^2 + C_y^2)^{3/2}} \quad (19)$$

External Energy Result: As stated before, a median filter has been employed in order to delete all the uniform part of the figure and to highlight the edges. It searches the 13th element of the 5×5 mask (Figure 5).

Once the median filter has been applied over the degrees image we apply and AND operation between it and the edges regions image so that we can highlight the points which result to be in overlay (Figure 6).

3.3 Post-processing

The image obtained from the previous steps present only the WBCs edges that, in some regions of the image, are far from being a connected boundary. Thus, a further step is needed to link the edges preserving the original boundary of the objects. Actually, this phase includes different steps. The first one

consists in connecting every single white point to the nearest in order to produce a connected objects boundary. A dilation with a 6 pixels size diamond structural element is applied in order to dilate all white dots. Secondly, the opening of the closing is applied with a 4 and 3 pixels size disks, respectively. Then, the skeleton function is performed. It produces an image that contains some spurious branches which are redundant for our purposes and, consequently, we realized the following strategy in order to get rid of them. To solve this problem we used a path analyser that checks for the presence of open paths. Indeed, a connected border is a closed path in which a pixel of that border is at the same time a starting and ending point. So, each pixel that does not belong to a closed path is removed. At this moment, every pure edge belonging to the cells is available but over-segmentation could occur so that we need to perform an arithmetical operation which fills all the WBCs edges and removes the others. This operation uses a mask obtained from the external force image. Finally, the application of an opening on the edge map with a 6 pixels radius disk structural element and its addition to WBCs image in foreground, all connected components, fitting into a specific area range, are successfully extracted, as shown in fig. 7. It is the first WBC segmented image obtained with the proposed method. It needs some improvements, following defined.

Once the cleaned binary mask has been obtained, we should be able to perform the count of the cells inside the image. Unfortunately, as it can be observed in Figure 8, using the proposed method also some WBCs have been separated in two or more regions, hampering a correct cell counting.

Thus, it is necessary a further step that merges all the image regions that belongs to the same cells. In order to understand which are the regions that should be part of a single cell we performed a check based on the area value. All the regions that have an area smaller than the half of the biggest region inside the
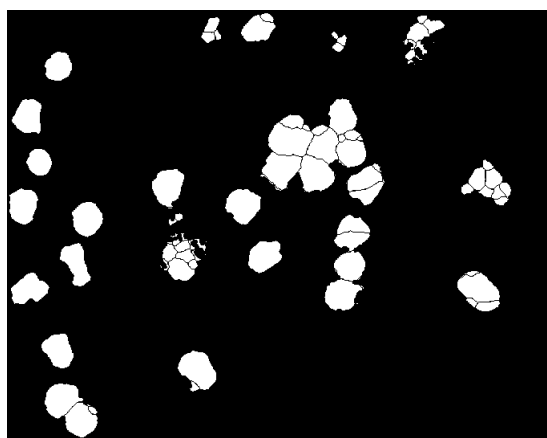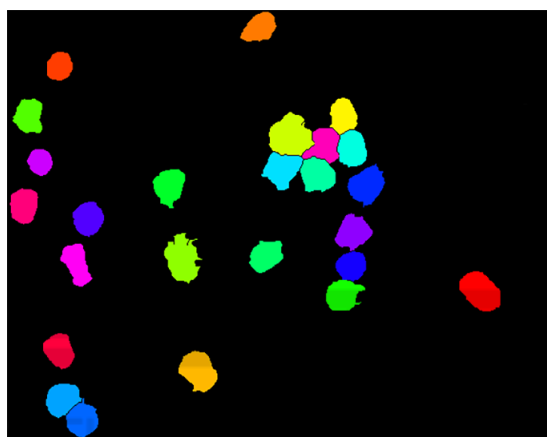
Figure 8: Oversegmented image.

Figure 9: Final result.

image are considered part of a single cell, while the other regions are considered complete cells. Keeping in mind that smaller area regions belong to larger area regions, we need to identify which of the first ones belongs to the latter. The threshold area used to create these two different images is exactly half of the image's biggest region area. Labelling each area and computing all the centroids, we can know which areas need to be joined together, using the Euclidean distance formula. Finally, it is possible to isolate the two areas and merge them using a closing procedure with a 7 pixels radius disk element. The final result is given by an overlay of this step to the over-segmented image by means of the union operator (figure 9).

4 DATASETS AND EXPERIMENTAL RESULTS

This section present the experimental result of the proposed white blood cells nuclei segmentation technique. The system has been tested on three different dataset, that is ALL-IDB, IUMS-IDB and SMC-IDB. First one is composed of images captured with an optical laboratory microscope coupled with a Canon PowerShot G5 camera. All the images are in JPG format with 24-bit colour depth. The first 33 have 1712×1368 resolution, while the remaining have 2592×1944 resolution. The images are taken with different magnifications of the microscope ranging from 300 to 500 which brings the colour differences that we managed grouping the images with same brightness characteristics together. It is composed of two versions: ALL-IDB1 and ALL-IDB2. ALL-IDB1 can be used for testing the segmentation capability of the algorithms. This dataset is composed of 108 images collected during September, 2005. It contains about 39000 blood elements, where the lymphocytes have been labelled by expert oncologists (Unimi, 2005). ALL-IDB2 has been designed for testing the performances of classification systems. The ALL-IDB2 version is a collection of cropped area of interest of healthy and blast cells that belong to the ALL-IDB1 dataset. They have similar grey level properties to ALL-IDB1 images, except from their dimensions (Unimi, 2005). In order to understand if the algorithm can obtain the best result with every kind of luminance or noise, it has been tested over two more datasets. IUMS-IDB is provided by Iran University of Medical Science (Sarrafzadeh et al., 2014) and contains 100 microscopic images of size 732×572, taken from peripheral blood of 8 healthy subjects. They are really different from those of ALL-IDB, since the microscope slides have been smeared and stained with a different staining technique. The third dataset, proposed in (Mohamed et al., 2012), has been acquired from slides stained with the same staining technique as ALL-IDB, even though the images are really different, since they have been acquired with a different combination of microscope and camera. It has a total of 367 peripheral blood images of size 640×480.

A visual result for each dataset is reported in fig. 10. A quantitative experimentation has been conducted by considering every single image for a WBCs analysis and relative count. Three metrics have been adopted to evaluate our study: False Negative Rate (FNR), Precision and Recall. The obtained results are reported in table 1. It is evident that our approach correctly identifies 100% of the leukocytes inside ALL-IDB, IUMS-IDB and SMC-IDB datasets. The majority of clumped cells has been found in ALL-IDB, which presents a lot of complex images, with lots of leukocytes per image and different agglomerates, while IUMS-IDB and SMC-IDB contain simpler images composed of fewer leukocytes and only few, sim-

Table 1: Detection performances compared with the state-of-the-art.

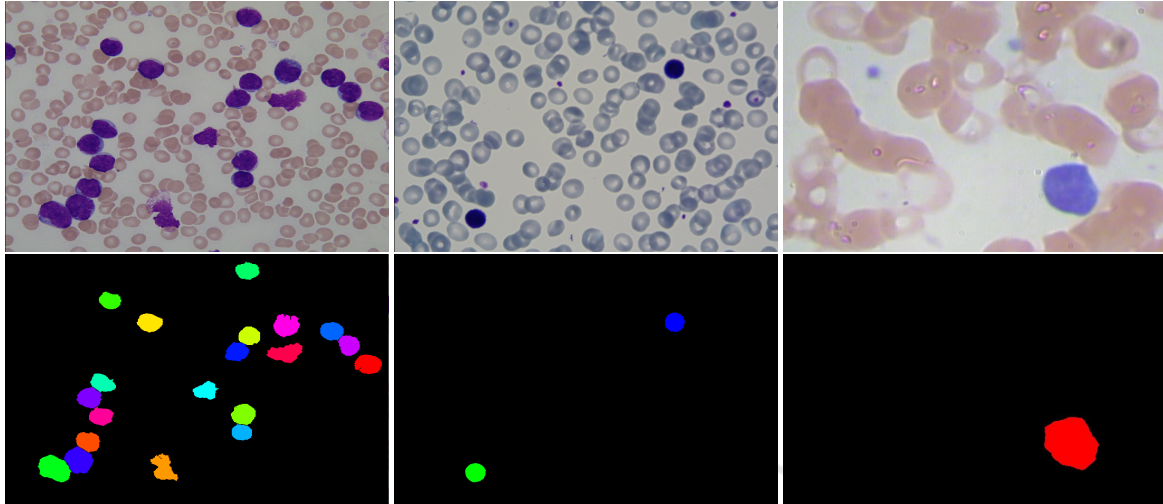| | Mahmood, 2013 | Alilou, 2013 | Putzu, 2014 | Alomari, 2014 | Di Ruberto, 2016 | | | Our Approach | | |
	ALL	ALL	ALL	ALL	ALL	IUMS	SMC	ALL	IUMS	SMC
FNR	-	-	-	1.5%	0.7%	0%	0%	0%	0%	0%
Precision	-	-	-	90%	100%	100%	100%	100%	100%	100%
Recall	81%	88%	92%	98%	99.2%	100%	100%	100%	100%	100%

Figure 10: Top: from left to right, images extracted from ALL-IDB, IUSMS-IDB and SMC-IDDB, respectively. Bottom: from left to right, the final segmentation results for each image on top.

pler, agglomerates. They also have a poorer quality than the ALL-IDB images. The proposed approach produces no false positives, being able to exclude all other image regions before the detection phase, and thus considering only the portions of image containing leukocytes. Some other state of the art methods used the aforementioned datasets for their segmentation clumped cells separation experiments, e.g. (Lata et al., 2016) and (Di Ruberto et al., 2015) use ALL-IDB. The first authors perform a WBCs count by counting the number of connected components even though it is not present a method to divide the clumped cells, while the second ones perform a separation of clumped and overlapped cells although they state some errors in the procedure. Our proposed approach outperforms both.

5 CONCLUSIONS

A new semi-automated WBCs recognition system has been investigated and proposed in this work. It can be used to support some existing medical methods, like the white blood cells counting. Its novelty in the state of the art is related to the clumped cells separation strategy, realised using a Vector Field Convolution model. It works by following only their na-

tural shape even if they are hard to distinguish. Its strength lies in the invariance to cells shapes and, by using the gradients movement, it can find the edge shape even if this is not immediately visible. Moreover, the proposed algorithm is not tuned to a specific training set and it could be used for whichever peripheral blood images dataset. Experimental results demonstrate that this new approach is very accurate and robust for detection, if compared to some traditional methods, being able to obtain excellent results with the three public tested datasets, even though some improvements could be implemented. Firstly, the post-processing phase could be afforded with an edge-linking algorithm referred the same region edges, in order to reduce the computational cost of this step. Secondly, the pre-processing step could be improved so as to consider both WBCs nuclei and cytoplasm.

REFERENCES

Alilou, M. and Kovalev, V. (2013). Automatic object detection and segmentation of the histocytology images using reshapable agents. *Image Analysis and Stereology*, 32(2):89–99.

Alomari, Y. M., Huda, S. A. S. N., Raja, Z. A., and Khairud-

din, O. (2014). Automatic detection and quantification of wbcs and rbcs using iterative structured circle detection algorithm. *Computational and mathematical methods in medicine*, 2014.

Bing, L. and Scott, T. (2007). Active contour external force using vector field convolution for image segmentation. *Acton, vol. 16, pp. 2096 - 2106*.

Di Ruberto, C., Loddo, A., and Putzu, L. (2015). a multiple classifier learning by sampling system for white blood cells segmentation. *proceedings in CAIP, vol. 9257, pp. 415 - 425*.

Di Ruberto, C., Loddo, A., and Putzu, L. (2016). A leucocytes count system from blood smear images. *Machine Vision and Applications, vol. 27, pp. 1151 - 1160*.

Gao, W., Yang, L., Zhang, X., and Liu, H. (2010). An improved sobel edge detection. *2010 3rd International Conference on Computer Science and Information Technology, pp. 67 - 71*.

Ghane, N., Vard, A., Talebi, A., and Nematollahy, P. (2017). Segmentation of white blood cells from microscopic images using a novel combination of k-means clustering and modified watershed algorithm. *ournal of Medical Signals and Sensors. vol. 7, no. 2, pp. 92-101*.

Halim, N. H. A., Mashor, M. Y., and Hassan, R. (2011). Automatic blasts counting for acute leukemia based on blood samples. *International Journal of Research and Reviews in Computer Science, vol. 2, no. 4*.

Kovalev, V. A., Y.Grigoriev, A., and H.Ahn (1996). Robust recognition of white blood cell images. *IEEE Publisher, pp. 371-375*.

Lata, A., Udesang, K. B., and Joshi, J. J. M. (2016). segmentation and counting of wbcs and rbcs from microscopic blood sample images. *proceedings in MECS (http://www.mecs-press.org/), vol. 11, pp. 32 - 40*.

Loddo, A., Putzu, L., Ruberto, C. D., and Fenu, G. (2016). A computer-aided system for differential count from peripheral blood cell images. In *2016 12th International Conference on Signal-Image Technology Internet-Based Systems (SITIS)*, pages 112–118.

Madhloom, H. T., Kareem, S. A., Ariffin, H., Zaidan, A. A., Alanazi, H. O., and Zaidan, B. B. (2010). An automated white blood cell nucleus localization and segmentation using image arithmetic and automated threshold. *Journal of Applied Sciences, vol. 10, no. 11, pp. 959-966*.

Mahmood, N. H., Lim, P. C., Mazalan, S. M., and Razak, M. A. A. (2013). Blood cells extraction using color based segmentation technique. *International Journal of Life Sciences Biotechnology and Pharma Research*, 2(2).

Mohamed, M., Far, B., and Guaily, A. (2012). An efficient technique for white blood cells nuclei automatic segmentation. *IEEE International Conference on Systems, Man, and Cybernetics (SMC), pp. 220225*.

Mohapatra, S., Patra, D., and Satpathy, S. (2013). An ensemble classifier system for early diagnosis of acute lymphoblastic leukemia in blood microscopic images. *Journal of Neural Computing and Applications, Article in Press,*.

Putzu, L., Caocci, G., and Di Ruberto, C. (2014). Leucocyte classification for leukaemia detection using image processing techniques. *Artificial Intelligence in Medicine, vol. 62 , pp. 179 - 191*.

Sarrafzadeh, O., Rabbani, H., Talebi, A., and Banaem, H. (2014). Selection of the best features for leukocytes classification in blood smear microscopic images. *SPIE Medical Imaging, pp. 90410P 90410P*.

Scotti, F. (2006). Robust segmentation and measurements techniques of white cells in blood microscope images. *IEEE Publisher, pp. 43-48*.

Scotti, F. and Piuri, V. (2004). Morphological classification of blood leucocytes by microscope images. *IEEE Publisher pp. 103-108*.

Sinha, N. and Ramakrishnan, A. G. (2003). Automation of differential blood count. in proceedings of the conference on convergent technologies for the asia-pacific region. *IEEE Publisher, vol. 2, pp. 547-551, Taj Residency, Bangalore*.

Unimi (2005). All-idb acute lymphoblastic leukemia image database for image processing.

Xu, C. and Prince, J. L. (1998). Generalized gradient vector flow external forces for active contours. *Signal Process., vol. 71, pp. 131 - 139*.